CEAS EuroGNC 2019
"Conference on Guidance, Navigation and Control"
3-5 April 2019 @ Politecnico di Milano, Milan, Italy.

CEAS-GNC-2019-020

Advanced Aeroelastic Robust Stability Analysis with Structural Uncertainties

Özge Süelözgen

Abstract Robust flutter analysis deals with aeroelastic (or aeroservoelastic) stability analysis taking structural dynamics, aerodynamics and/or unmodeled system dynamics uncertainties into account. Flutter is a well-known dynamic aeroelastic instability phenomenon caused by an interaction between structural vibrations and unsteady aerodynamic forces, whereby the level of vibration may trigger large amplitudes, eventually leading to catastrophic failure of the structure. This paper addresses the issue of an approach for aeroelastic robust stability analysis with structural uncertainties with respect to physical symmetric and asymmetric stiffness perturbations on the wing structure by means of tuning beams.

1 Introduction

The primary aim of this paper is to investigate the impact of the stiffness uncertainties of the wings in spanwise direction and handle each wing seperately in case of symmetric and especially asymmetric stiffness distribution. It is quite possible that poor levels of precision with respect to manufacturing capabilities a small difference of bending and/or torsional stiffness may occur between the two wing structures which -in worst case scenario- can be significant enough to cause an unpredictable coupling between symmetric and asymmetric modes. Therefore, it is essential to model such an asymmetry by means of a adequate uncertainty in physical stiffness model for each wing separately. In this context a linear fractal transformation (LFT) model of the perturbed aeroelastic system in the time domain state-space framework is developed for the robust flutter analysis.

German Aerospace Center (DLR) - Institute of System Dynamics and Control, 82234 Wessling-Germany, e-mail: oezge.sueeloezgen@dlr.de

2 Linear fractional transformation and μ -Analysis

The linear fractional transformation (LFT) is a common framework for robust stability analysis of complex systems based on the small gain theorem [1]. An LFT is an interconnection of operators arranged in a feedback manner. Let be $\mathbf{P}$ a linear complex operator partitioned as

$$\mathbf{P} = \begin{bmatrix} \mathbf{P_{11}} & \mathbf{P_{12}} \\ \mathbf{P_{21}} & \mathbf{P_{22}} \end{bmatrix} \quad \in \quad \mathbb{C}^{(o_1+o_2)\ x\ (i_1+i_2)} \tag{1}$$

The LFT, $\mathbf{F_u}(\mathbf{P}, \mathbf{\Delta})$ is defined as the closed-loop transfer matrix from system input u to system output y as the upper-loop LFT of system $\mathbf{P}$ closed by $\mathbf{\Delta}$:

$$\mathbf{F_u}(\mathbf{P}, \mathbf{\Delta}) = \mathbf{P_{22}} \ + \ \mathbf{P_{21}}\mathbf{\Delta}(\mathbf{I} - \mathbf{P_{11}}\mathbf{\Delta})^{-1}\mathbf{P_{12}} \tag{2}$$

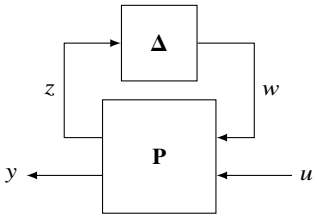

Fig. 1 Upper-LFT formulation of the perturbated system

An equivalent expression $\mathbf{F_l}(\mathbf{P}, \mathbf{\Delta})$ is defined as the closed-loop transfer matrix from system input u to system output y as the lower-loop LFT of system $\mathbf{P}$ closed by $\mathbf{\Delta}$:

$$\mathbf{F_l}(\mathbf{P}, \mathbf{\Delta}) = \mathbf{P_{11}} \ + \ \mathbf{P_{12}}\mathbf{\Delta}(\mathbf{I} - \mathbf{P_{22}}\mathbf{\Delta})^{-1}\mathbf{P_{21}} \tag{3}$$

It can be seen from the Equation (2) that $\mathbf{P_{22}}$ denotes the transfer function (matrix) from input u to output y of the nominal plant while $\mathbf{P_{11}}$, $\mathbf{P_{12}}$ and $\mathbf{P_{21}}$ content the information how the perturbation is embedded in the nominal plant. After the uncertainty block $\mathbf{\Delta}$ is extracted from the nominal plant, the system can be described as a nominal plant with an *artificial* feedback-loop. From the equation (2) it becomes apparent that the LFT is well-posed if and only if the inverse of $(\mathbf{I} - \mathbf{P_{11}}\mathbf{\Delta})$ exist.

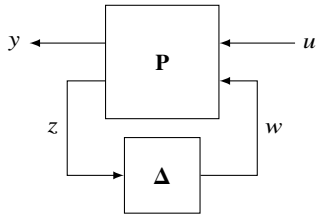

Fig. 2 Lower-LFT formulation of the perturbated system

3 Structured Singular Value μ

The structured singular value μ is an exact indicator of robust stability for systems with structured uncertainties (perturbations). It is a function of the complex transfer function matrix $\mathbf{P}$ where $\mathbf{\Delta}$ is the norm-bounded structured matrix of perturbations and $\bar{\sigma}(\cdot)$ deneotes the maximum singular value of the argument

$$\mu(\mathbf{P}) = \frac{1}{\min\limits_{\Delta \in \mathbf{\Delta}} \{\bar{\sigma}(\Delta) \ : \ \det(\mathbf{I} - \mathbf{P}\Delta) \ = \ 0\}} \tag{4}$$

$$\forall \Delta \in \mathbf{\Delta} \text{ such that } \det(\mathbf{I} - \mathbf{P}\Delta) = 0 \text{ otherwise } \mu = 0$$

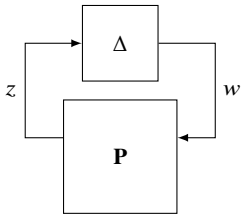

Fig. 3 LFT system for robust stability analysis using in μ-Framework

In this context $\mathbf{P}$ is robustly stable with respect to Δ which is norm-bounded by scalar $\beta \in \mathbb{R}$ such that $\|\tilde{\Delta}\|_\infty \leq \beta, \ \forall \tilde{\Delta} \in \Delta$ if and only if $\mu(\mathbf{P}) \leq \frac{1}{\beta}$. In the μ-framework the model $\mathbf{P}$ is usually weighted to normalize the norm-bounded uncertainty set Δ to unity

$$\|\Delta\|_\infty \leq 1, \ \forall \Delta \in \mathbf{\Delta} \quad \text{if and only if} \quad \mu(\mathbf{P}) \leq 1 \tag{5}$$

For $\mu \leq 1$ there is no perturbation within exists that will destabilize the system. This state depicts that the *true* system dynamics are stable, assumming the nomimal model dynamics with its set of uncertainty operators (modeling errors) are able to capture the dynamic behaviour of the *true* system.

4 Aeroelastic Model

In this paper a condensed FE model of the FLEXOP demonstrator aircraft [2] for the numerical demonstration of the robust flutter analysis is used. The full FE model (> 600000 nodes) comprises the wing, fuselage and empennage. The wing is modeled by a high-fidelity FE model comprising beam, surface and solid elements. The condensation of the FE model has been performed by the Guyan-reduction, also known as static condensation. The reduced model consists of 303 structural nodes and 1818 degrees of freedom (DoF). The aerodynamic model is based on vortex lattice method (VLM) for steady aerodynamics and doublet lattice method (DLM) for unsteady aerodynamics. A detailed overview of both the structural and aerodynamic model of the aircraft is described in [2].

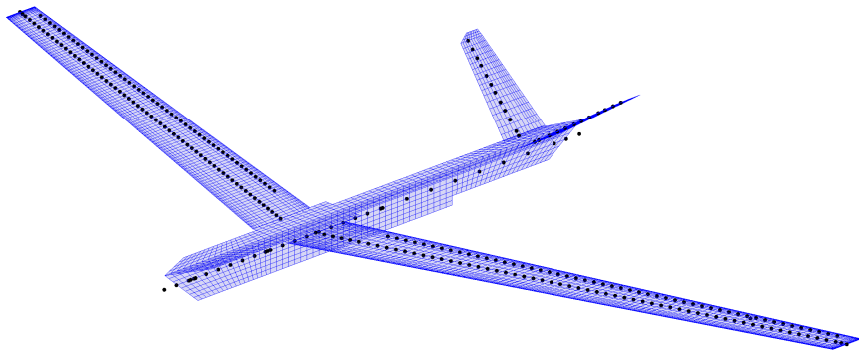

Fig. 4 Aerodynamic panel model of the FLEXOP aircraft and structural nodes of condensed FE model

4.1 Equations of motion for the aeroelastic system

The equations of motion for the nominal aeroelastic system in time domain can expressed in a matrix form as

$$\mathbf{M}\ddot{x}(t) + \mathbf{C}\dot{x}(t) + \mathbf{K}x(t) = \frac{1}{2}\rho V^2 \mathbf{A}(\bar{s}, Ma)x(t) = P^{aero}(t) \tag{6}$$

which describes a system of N linear ordinary differential equations with N degrees of freedom (DoF) in the FE model where $x(t)$ is the displacement vector with

translational and rotational DoFs of the nodes, $\mathbf{M}$, $\mathbf{K}$ and $\mathbf{C} \in \mathbb{R}^{N\ x\ N}$ are physical mass, stiffness and viscous damping matrices respectively belonging to the structural dynamics part of the equation. The right hand side of the equation (6) denotes the unsteady aerodynamic forces where ρ is the density of atmosphere, V is the flight speed and $\mathbf{A}(\bar{s}, Ma)$ is the unsteady aerodynamic influence coefficient (AIC) matrix which is a function of nondimensional Laplace variable $\bar{s}$ and the Mach number Ma. The AIC matrix can be computed by several aerodynamic theories, such as doublet lattice method (DLM). In this paper, the subsonic unsteady aerodynamic forces have been modeled by means of DLM. Based on small disturbance hypothesis, DLM solves the linearized potential flow equation and obtains the aerodynamic forces under the assumption that aerodynamic surfaces oscillate harmonically. The nondimensional Laplace variable $\bar{s}$ is denoted $\bar{s} = g + ik$ where g is the damping and k is the reduced frequency. On the assumption of harmonic aerodynamic loads the nondimensional Laplace variable $\bar{s}$ becomes:

$$\bar{s} = s\frac{c_{ref}}{2V} = i\omega\frac{c_{ref}}{2V} = ik \tag{7}$$

where ω is the frequency of vibration, c_{ref} is the reference chord. Note that the dependence on the Mach number of the AIC matrix will be omitted from now on for conciseness.

Using mode displacement method the physical displacement vector $x(t)$ can be represented as a linear combination of m linearly independent vectors (mode shapes) leading to the approximation

$$x(t) = \mathbf{\Phi}\eta\ , \quad \mathbf{\Phi} = \left[\Phi_1\ \Phi_2\ \ldots \Phi_m\right]\ \in\ \mathbb{R}^{N\ x\ m} \tag{8}$$

where m is the number of eigenvectors.

Combination of the Equations (6), (8) and (7) results in the following reduced-order dynamics

$$\mathbf{M}_m\ddot{\eta}(t) + \mathbf{B}_m\dot{\eta}(t) + \mathbf{K}_m\eta(t) = \frac{1}{2}\rho V^2\mathbf{A}_m(ik)\eta(t) = P_m^{aero}(t) \tag{9}$$

with

$$\mathbf{M}_m = \mathbf{\Phi}^T\mathbf{M}\mathbf{\Phi} \tag{10}$$

$$\mathbf{B}_m = \mathbf{\Phi}^T\mathbf{C}\mathbf{\Phi} \tag{11}$$

$$\mathbf{K}_m = \mathbf{\Phi}^T\mathbf{K}\mathbf{\Phi} \tag{12}$$

$$\mathbf{A}_m(ik) = \mathbf{\Phi}^T\mathbf{A}(ik)\mathbf{\Phi} \tag{13}$$

where $\mathbf{M}_m$ is the generalized mass matrix, $\mathbf{C}_m$ is the generalized viscous damping matrix, $\mathbf{K}_m$ is the generalized stiffness matrix and $\mathbf{A}_m(ik)$ is the generalized AIC matrix.

4.2 Rational Function Approximation

The generalized AIC matrix $\mathbf{A}_m(ik) \in \mathbb{C}^{m\ x\ m}$ is a set of matrices which are calculeted for a set of suitable values of reduced frequency k. Thus, in order to compute AIC for any desired reduced frequency point and perform time domain analysis (state-space representation), the AIC matrix in frequency-domain has to be transformed into the Laplace domain and consequently into the time domain. A possible way is to fit the frequency dependent AIC matrix with rational functions in a least-squares sense. This method is called Rational Function Approximation (RFA) [3]. In this paper the Roger's formulation is used to approximate the AIC matrix $\mathbf{A}_m(ik)$:

$$\mathbf{A}_m(ik) = \mathbf{A}_m(\bar{s}) \ \approx \ \mathbf{A}_m^0 + \bar{s}\mathbf{A}_m^1 + \bar{s}^2\mathbf{A}_m^2 \ + \ \sum_{i=1}^{n_p} \mathbf{A}_m^{L_i} \frac{\bar{s}}{\bar{s} + \beta_i} \tag{14}$$

The RFA equation (14) can be interpreted as a general two-part approach for aeroldynamic loads based on quasi-staedy and lag contributions. $\mathbf{A}_m^0$, $\mathbf{A}_m^1$ and $\mathbf{A}_m^2$ are $\mathbb{R}^{m\ x\ m}$ real coefficient matrices representing the contribution of acceleration, velocity and dispalecement of the flexible/rigid degrees of the freedom on the aerodynamic loads denoting the quasi-staedy part of the approximation. The $\mathbf{A}_m^{L_i} \in \mathbb{R}^{m\ x\ m}$ matrices with the predefined poles $\beta_i,\ i = 1, 2, ..., n_p$, are responsible for the lagging behavior of the unsteady flow. This is referred to *time lag effect*.

For time domian respresentation the equation system in (14) can be rearranged as follows

$$\mathbf{A}_m(\bar{s}) \ \approx \ \mathbf{A}_m^0 + \bar{s}\mathbf{A}_m^1 + \bar{s}^2\mathbf{A}_m^2 + \mathbf{D}(\bar{s}\mathbf{I} - \mathbf{R})^{-1}\mathbf{E}\bar{s} \tag{15}$$

where

$$\mathbf{D} = \begin{bmatrix} \mathbf{A}_m^{L_1} & \mathbf{A}_m^{L_2} & \dots & \mathbf{A}_m^{L_{n_p}} \end{bmatrix} \in \mathbb{R}^{m\ x\ (m \cdot n_p)} \tag{16}$$

$$\mathbf{R} = diag\left(\begin{bmatrix} -\beta_1\mathbf{I} & -\beta_2\mathbf{I} & \dots & -\beta_{n_p}\mathbf{I} \end{bmatrix}\right) \in \mathbb{R}^{(m \cdot n_p)\ x\ (m \cdot n_p)} \tag{17}$$

$$\mathbf{E} = \begin{bmatrix} \mathbf{I} & \mathbf{I} & \dots & \mathbf{I} \end{bmatrix}^T \in \mathbb{R}^{(m \cdot n_p)\ x\ m} \tag{18}$$

For the lag states $x_L \in \mathbb{R}^{n_{lag}\ x\ 1}$ following ordinary differential equation (ODE) with $\dot{\eta}$ as input can be derived [3]:

$$\dot{x}_L \ = \ \left(\frac{V}{c_{ref}/2}\right) \mathbf{R}x_L + \mathbf{E}\dot{\eta} \tag{19}$$

The resulting generalized aerodynamic forces are then

$$P_m^{aero} = \frac{1}{2}\rho V^2 \mathbf{A}_m(ik)\eta(t) \approx \frac{1}{2}\rho V^2 \left(\mathbf{A}_m^0 \eta + \frac{c_{ref}/2}{V}\mathbf{A}_m^1 \dot{\eta} + \left(\frac{c_{ref}/2}{V}\right)^2 \mathbf{A}_m^2 \ddot{\eta} + \mathbf{D}x_L \right) \tag{20}$$

5 LFT model of the pertubated system

Consider again the generalized equations of motion for the aeroelastic response of the aircraft with unstaedy aerodynamics by combining the equation (9) and (20)

$$\mathbf{M}_m\ddot{\eta}(t)+\mathbf{B}_m\dot{\eta}(t)+\mathbf{K}_m\eta(t) = \frac{1}{2}\rho V^2 \left(\mathbf{A}_m^0 \eta + \frac{c_{ref}/2}{V}\mathbf{A}_m^1 \dot{\eta} + \left(\frac{c_{ref}/2}{V}\right)^2 \mathbf{A}_m^2 \ddot{\eta} + \mathbf{D}x_L \right) \tag{21}$$

The state-space respresentation of the Equation (21) is formulated with the generalized states η, $\dot{\eta}$ and the unsteady aerodynamic states x_L:

$$\begin{bmatrix} \dot{\eta} \\ \ddot{\eta} \\ \dot{x}_L \end{bmatrix} = \begin{bmatrix} \mathbf{0} & \mathbf{I} & \mathbf{0} \\ -(\mathbf{M}_m^A)^{-1}\mathbf{K}_m^A & -(\mathbf{M}_m^A)^{-1}\mathbf{C}_m^A & \frac{1}{2}\rho V^2 (\mathbf{M}_m^A)^{-1}\mathbf{D} \\ \mathbf{0} & \mathbf{E} & \frac{2V}{c_{ref}}\mathbf{R} \end{bmatrix} \begin{bmatrix} \eta \\ \dot{\eta} \\ x_L \end{bmatrix} \tag{22}$$

where

$$\mathbf{M}_m^A = \mathbf{M_m} - \rho\frac{c_{ref}^2}{8}\mathbf{A}_m^2 \tag{23}$$

$$\mathbf{K}_m^A = \mathbf{K}_m - \frac{1}{2}\rho V^2 \mathbf{A}_m^0 \tag{24}$$

$$\mathbf{C}_m^A = \mathbf{C}_m - \frac{c_{ref}}{4}\rho V \mathbf{A}_m^1 \tag{25}$$

5.1 Parametrization over flight speed

The μ-framework determines the stability over a range of airspeed to specify the onset of flutter. The generalized equations of motion for the aeroelastic response (22) is a function of the flight speed V so that perturbations of this parameter can be integrated into the system as a linear fractional transformation.

Consider an additive perturbation, δV, on the nominal velocity, $\bar{V}$

$$V = \bar{V} + \delta V \tag{26}$$

Separate terms in the system dynamics (22) that involve δV:

$$\left[\begin{array}{c} \dot{\eta} \\ \ddot{\eta} \\ \dot{x}_L \\ \hline \mathbf{z}_V \end{array}\right] = \left[\begin{array}{c|c} \bar{\mathbf{A}} & \bar{\mathbf{B}}_V \\ \hline \bar{\mathbf{C}} & \bar{\mathbf{D}}_V \end{array}\right] \left[\begin{array}{c} \eta \\ \dot{\eta} \\ x_L \\ \hline \mathbf{w}_V \end{array}\right] \tag{27}$$

where

$$\bar{\mathbf{A}} = \begin{bmatrix} \mathbf{0} & \mathbf{I} & \mathbf{0} \\ -(\mathbf{M}_m^A)^{-1}\left(\mathbf{K}_m - \frac{1}{2}\rho\bar{V}^2\mathbf{A}_m^0\right) & -(\mathbf{M}_m^A)^{-1}\left(\mathbf{C}_m - \frac{c_{ref}}{4}\rho\bar{V}\mathbf{A}_m^1\right) & \frac{1}{2}\rho\bar{V}^2(\mathbf{M}_m^A)^{-1}\mathbf{D} \\ \mathbf{0} & \mathbf{E} & \frac{2\bar{V}}{c_{ref}}\mathbf{R} \end{bmatrix} \tag{28}$$

$$\bar{\mathbf{B}}_V = \begin{bmatrix} \mathbf{0} & \mathbf{0} & \mathbf{0} & \mathbf{0} \\ \bar{V}\mathbf{I} & \mathbf{0} & \bar{V}\mathbf{I} & \mathbf{I} \\ \mathbf{0} & \mathbf{I} & \mathbf{0} & \mathbf{0} \end{bmatrix} \tag{29}$$

$$\bar{\mathbf{C}} = \begin{bmatrix} \frac{1}{2}\rho(\mathbf{M}_m^A)^{-1}\mathbf{A}_m^0 & \mathbf{0} & \mathbf{0} \\ \mathbf{0} & \mathbf{0} & \frac{2}{c_{ref}}\mathbf{R} \\ \mathbf{0} & \mathbf{0} & \frac{1}{2}\rho(\mathbf{M}_m^A)^{-1}\mathbf{D} \\ \frac{1}{2}\rho\bar{V}(\mathbf{M}_m^A)^{-1}\mathbf{A}_m^0 & \frac{c_{ref}}{4}\rho(\mathbf{M}_m^A)^{-1}\mathbf{A}_m^1 & \frac{1}{2}\rho\bar{V}(\mathbf{M}_m^A)^{-1}\mathbf{D} \end{bmatrix} \tag{30}$$

$$\bar{\mathbf{D}}_V = \begin{bmatrix} \mathbf{0} & \mathbf{0} & \mathbf{0} & \mathbf{0} \\ \mathbf{0} & \mathbf{0} & \mathbf{0} & \mathbf{0} \\ \mathbf{0} & \mathbf{0} & \mathbf{0} & \mathbf{0} \\ \mathbf{I} & \mathbf{0} & \mathbf{I} & \mathbf{0} \end{bmatrix} \tag{31}$$

The additional input and outputs signals, $\mathbf{w}_V = [w_1, w_2, w_3, w_4]^T$ and $\mathbf{z}_V = [z_1, z_2, z_3, z_4]^T$, are introduced into nominal aeroelastic system given in (22) to include the perturbation in velocity to the nominal dynamics in a feedback manner:

$$z_1 = \frac{\rho}{2}(\mathbf{M}_m^A)^{-1}\mathbf{A}_m^0\eta \tag{32}$$

$$z_2 = \frac{2}{c_{ref}}\mathbf{R}x_L \tag{33}$$

$$z_3 = \frac{\rho}{2}(\mathbf{M}_m^A)^{-1}\mathbf{D}x_L \tag{34}$$

$$z_4 = \frac{\rho}{2}\bar{V}(\mathbf{M}_m^A)^{-1}\mathbf{A}_m^0\eta + \frac{c_{ref}}{4}\rho(\mathbf{M}_m^A)^{-1}\mathbf{A}_m^1\dot{\eta} + \frac{\rho}{2}\bar{V}(\mathbf{M}_m^A)^{-1}\mathbf{D}x_L + w_1 + w_3 \quad (35)$$

$$\mathbf{w}_V = \delta V \mathbf{z}_V \quad (36)$$

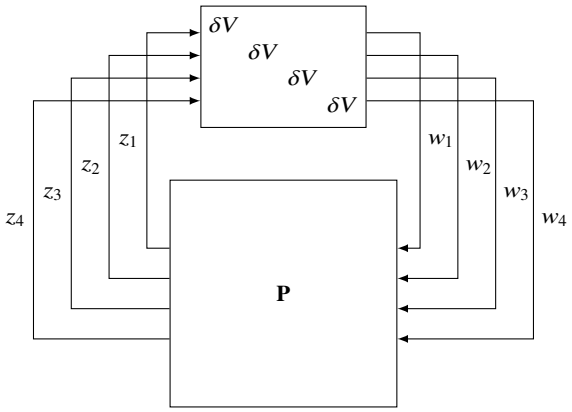

Fig. 5 Upper-LFT system for nominal stability analysis in μ-framework with perturbation in flight speed

The nominal flutter problem modeled by means of perturbation to flight speed V in equation (27) can be solved as a μ computation. The tranfer function matrix $\mathbf{P}(s)$ which relates the input signal $\mathbf{w}_V$ to the output signal $\mathbf{z}_V$ can be derived from the equation (27):

$$\mathbf{P}(s) = \bar{\mathbf{C}}\left(s\mathbf{I} - \bar{\mathbf{A}}\right)^{-1}\bar{\mathbf{B}}_V + \bar{\mathbf{D}}_V \quad (37)$$

To make the perturbation on flight speed δV which has the same unit as $\bar{V}$, to unity norm-bound constraint $\|\delta V\|_\infty \leq 1$, the transfer function matrix $\mathbf{P}(s)$ has to be scaled by a weighting $W_{\bar{V}}$, where

$$V = \bar{V} + \delta V \cdot W_{\bar{V}}, \quad \|\delta V\|_\infty \leq 1 \quad (38)$$

The scaled plant transfer function matrix $\bar{\mathbf{P}}(s)$ is given by:

$$\bar{\mathbf{P}}(s) = W_{\bar{V}}\mathbf{P}(s) \quad (39)$$

Now the nominal flutter speed $V_{flutter}^{nom}$ can be determined via μ computation by means of following algoritm.

Algorithm 1 Algoritm for nominal flutter margin within μ-framework

- Define initial weighting $W_{\bar{V}}$ for flight speed
- Determine $\bar{\mathbf{P}}(s)$ and calculate $\mu(\bar{\mathbf{P}})$
- Set tolerance value tol for exit condition

while $\mu(\bar{\mathbf{P}}) > 1 + tol$ OR $\mu(\bar{\mathbf{P}}) < 1 - tol$

$W_{\bar{V}} = W_{\bar{V}} / \mu(\bar{\mathbf{P}})$

$\bar{\mathbf{P}}(s) = W_{\bar{V}} \mathbf{P}(\mathbf{s})$

end

$V_{flutter}^{nom} = \bar{V} + W_{\bar{V}}$

The nominal flutter speed $V_{flutter}^{nom}$ can also be calculated by means of standard methods such as p-method, pk-method or g-method. The algoritm set out above should therefore give an introduction into the μ-framework.

For the robust aeroelastic stability analysis additional uncertainties such as in structural dynamics, aerodynamics and/or unmodelled system dynamics have to be defined and subsequently included into the linear system to introduce modeling errors between the numerical model and the physical aircraft.

6 Uncertainty Modeling

In this paper account is taken of the uncertainties in the structural dynamics or, more explicitly, the structural stiffness model which has a significant impact within the lower frequency range and flutter analysis respectively. For the realization of the stiffness parameter variations tuning beams have been generated with respect to the condensed FE model. This approach is suitable for varying of stiffness parameters by only adjusting material properties of the tuning beams like bending and torisonal stiffness avoiding to intervene the full FE model. In this study the wing structure is affected by the uncertainty of the physical stiffness matrix by means of tuning beams' parameters. Two kinds of variations of physical stiffness characteristics have been defined. The first approach is characterized by symmetric variation of physical stiffness with respect to torsional rigidity (GI_p) and/or flexural rigidity (bending stiffness) (EI_{xx}), i.e. the tuning beams on the right and left wing structure have the same material properties in order to include symmetric uncertainties into the nominal model. The second approach denotes asymmetric variation of stiffness parameters of the tuning beams on the right and left wing structure to represent asymmetric stiffness distribution in the nominal model.

Considering the perturbation of physical stiffness matrix of the aircraft, the parametric additive uncertainties can be described as follows:

I. Symmetric variation

$$\mathbf{K}_m^{sym} = \mathbf{\Phi}^T \left[\bar{\mathbf{K}} + \sum_{i=1}^{n_{beam}/2} \delta_i^W \left(\mathbf{K}_i^{WR} + \mathbf{K}_i^{WL} \right) \right] \mathbf{\Phi} \tag{40}$$

II. Asymmetric variation

$$\mathbf{K}_m^{asym} = \mathbf{\Phi}^T \left[\bar{\mathbf{K}} + \sum_{i=1}^{n_{beam}/2} \delta_i^{WR} \mathbf{K}_i^{WR} + \sum_{i=1}^{n_{beam}/2} \delta_i^{WL} \mathbf{K}_i^{WL} \right] \mathbf{\Phi} \tag{41}$$

where n_{beam} is the total number of tuning beams, $\bar{\mathbf{K}}$ is the nominal physical stiffness matrix, $\mathbf{K}_i^{WR}$ and $\mathbf{K}_i^{WR}$ are weigthing matrices which are in this case the physical stiffness matrices of the i^{th} tuning beam with respect to the right wing (WR) and left wing (WL) structure, respectively. δ_i, δ_i^{WR} and δ_i^{WL} are norm-bounded uncertainty operators with $\|\delta_i^W\|_\infty \leq 1$, $\|\delta_i^{WR}\|_\infty \leq 1$ and $\|\delta_i^{WL}\|_\infty \leq 1$. It should be noted that $\mathbf{\Phi}$ is the modal (eigenvector) matrix of the nominal system. This assumption is reasonable for small perturbations and can be validated by modal correlation analysis between nominal and perturbated system.

The extended LFT model of the new perturbated system, which includes feedback signals relating the perturbation to flight speed and the uncertainties described in the equations (40) and (41) may be defined analogous to the equation (27):

$$\left[\begin{array}{c} \dot{\eta} \\ \ddot{\eta} \\ \dot{x}_L \\ \hline \mathbf{z}_V \\ \mathbf{z}_K \end{array}\right] = \left[\begin{array}{c|c} \bar{\mathbf{A}} & \begin{bmatrix} \bar{\mathbf{B}}_V & \bar{\mathbf{B}}_K \end{bmatrix} \\ \hline \begin{bmatrix} \bar{\mathbf{C}} \\ \bar{\mathbf{C}}_K \end{bmatrix} & \begin{bmatrix} \bar{\mathbf{D}}_V & \bar{\mathbf{D}}_{V,K} \\ \bar{\mathbf{D}}_{K,V} & \bar{\mathbf{D}}_K \end{bmatrix} \end{array}\right] \left[\begin{array}{c} \eta \\ \dot{\eta} \\ x_L \\ \hline \mathbf{w}_V \\ \mathbf{w}_K \end{array}\right] \tag{42}$$

where the new submatrices are

$$\bar{\mathbf{B}}_K = \begin{bmatrix} \mathbf{0}_m & \mathbf{0}_m & \cdots & \mathbf{0}_m \\ -\mathbf{I}_m & -\mathbf{I}_m & \cdots & -\mathbf{I}_m \\ & \mathbf{0}_{n_{lag}\ x\ m \cdot n_{beam}} & & \end{bmatrix} \quad \in \mathbb{R}^{(2m+n_{lag})\ x\ (m \cdot n_{beam})} \tag{43}$$

$$\bar{\mathbf{C}}_K = \begin{bmatrix} (\mathbf{M}_m^A)^{-1}\mathbf{\Phi}^T\mathbf{K}_1^{WR}\mathbf{\Phi} & \mathbf{0}_m & \mathbf{0}_{m\ x\ n_{lag}} \\ \vdots & \vdots & \vdots \\ (\mathbf{M}_m^A)^{-1}\mathbf{\Phi}^T\mathbf{K}_{n_{beam}/2}^{WR}\mathbf{\Phi} & \mathbf{0}_m & \mathbf{0}_{m\ x\ n_{lag}} \\ (\mathbf{M}_m^A)^{-1}\mathbf{\Phi}^T\mathbf{K}_1^{WL}\mathbf{\Phi} & \mathbf{0}_m & \mathbf{0}_{m\ x\ n_{lag}} \\ \vdots & \vdots & \vdots \\ (\mathbf{M}_m^A)^{-1}\mathbf{\Phi}^T\mathbf{K}_{n_{beam}/2}^{WL}\mathbf{\Phi} & \mathbf{0}_m & \mathbf{0}_{m\ x\ n_{lag}} \end{bmatrix} \in \mathbb{R}^{(m\cdot n_{beam})\ x\ (2m+n_{lag})} \tag{44}$$

The submatrices $\bar{\mathbf{D}}_{V,K} \in \mathbb{R}^{(3m+n_{lag})x(3m+n_{lag})}$, $\bar{\mathbf{D}}_{K,V} \in \mathbb{R}^{(m\cdot n_{beam})x(3m+n_{lag})}$ and $\bar{\mathbf{D}}_K \in \mathbb{R}^{(m\cdot n_{beam})x(m\cdot n_{beam})}$ are zeros matrices.

The robust flutter problem modeled by means of perturbation to flight speed V and stiffness model uncertainty in equation (42) can be solved as a μ computation. The tranfer function matrix $\mathbf{P}_K(s)$ which relates the input signals $\mathbf{w}_V$ and $\mathbf{w}_K$ to the output signals $\mathbf{z}_V$ and $\mathbf{z}_K$ can be derived from the equation (42):

$$\mathbf{P}_K(s) = \begin{bmatrix} \bar{\mathbf{C}} \\ \bar{\mathbf{C}}_K \end{bmatrix} \left(s\mathbf{I} - \bar{\mathbf{A}}\right)^{-1} \begin{bmatrix} \bar{\mathbf{B}}_V & \bar{\mathbf{B}}_K \end{bmatrix} + \begin{bmatrix} \bar{\mathbf{D}}_V & \bar{\mathbf{D}}_{V,K} \\ \bar{\mathbf{D}}_{K,V} & \bar{\mathbf{D}}_K \end{bmatrix} \tag{45}$$

Once the tranfer function matrix $\mathbf{P}_K(s)$ has been determined the robust flutter speed $V_{flutter}^{rob}$ can be determined within the μ-framework work by means of following algoritm.

Algorithm 2 Algoritm for robust flutter margin within μ-framework

- Define initial weighting $W_{\bar{V}}$ for flight speed, for instance $W_{\bar{V}} = V_{flut}^{nom} - \bar{V}$
- Define a suitable frequency range $\omega = \omega_1, \ \ldots, \ \omega_{N_f}$
- Scale transfer function matrix $\mathbf{P_K}(s)$ with $\bar{\mathbf{P}}_K(s) = \begin{bmatrix} W_{\bar{V}} & \\ & \mathbf{I} \end{bmatrix} \mathbf{P}_K(s)$
- Compute $\mu(\bar{\mathbf{P}}_K(i\omega))$ with $s = i\omega$
- Set tolerance value tol for exit condition

while $\|1 - \max(\mu(\bar{\mathbf{P}}_K))\| > tol$

$W_{\bar{V}} = W_{\bar{V}}/\mu(\bar{\mathbf{P}})$

$\bar{\mathbf{P}}_K(s) = \begin{bmatrix} W_{\bar{V}} & \\ & \mathbf{I} \end{bmatrix} \mathbf{P}_K(s)$

end

$V_{flutter}^{rob} = \bar{V} + W_{\bar{V}}$

7 Numerical Results

For the numerical demonstration of the proposed uncertainty description 11 tuning beams for each wing ($n_{beam} = 22$) have been defined. Each wing consists of 60 structural nodes. The beams are placed within the nondimensional span range $\xi = [0.25,\ 0.75]$. For the modal model the first 15 modes ($m = 15$) have been consiered within the frequency range $2.9Hz \leq f \leq 35.6Hz$ where following case studies have been performed.

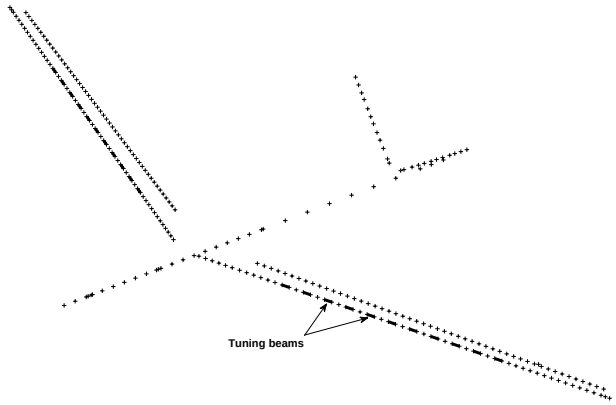

Fig. 6 Structural nodes of condensed FE model with the tuning beams

Symmetric stiffness perturbations

I Additive uncertainty of $10^2 \frac{N}{m^2}$ with respect to bending stiffness EI_{xx} for each tuning beam on the left and right wing structure

$$\mathbf{\Delta_K^I} = \text{diag}(\delta_1^W \mathbf{I_m},\ \delta_2^W \mathbf{I_m},\ \cdots,\ \delta_{\mathbf{n_{beam}/2}}^{\mathbf{W}} \mathbf{I_m})$$

II Additive uncertainty of $10^2 \frac{N}{m^2}$ with respect to torisonal stiffness GI_p for each tuning beam on the left and right wing structure

$$\mathbf{\Delta_K^{II}} = \text{diag}(\delta_1^W \mathbf{I_m},\ \delta_2^W \mathbf{I_m},\ \cdots,\ \delta_{\mathbf{n_{beam}/2}}^{\mathbf{W}} \mathbf{I_m})$$

III Additive uncertainty of $10^2 \frac{N}{m^2}$ with respect to both bending stiffness EI_{xx} and torisonal stiffness GI_p for each tuning beam on the left and right wing structure

$$\mathbf{\Delta_K^{III}} = \begin{bmatrix} \mathbf{\Delta_K}^{WR} & \\ & \mathbf{\Delta_K}^{WL} \end{bmatrix} \text{ where}$$
$$\mathbf{\Delta_K}^{WR} = \text{diag}(\delta_1^{WR}\mathbf{I_m},\ \delta_2^{WR}\mathbf{I_m},\ \cdots,\ \delta^{\mathbf{WR}}_{\mathbf{n_{beam}/2}}\mathbf{I_m}) \text{ and}$$
$$\mathbf{\Delta_K}^{WL} = \text{diag}(\delta_1^{WL}\mathbf{I_m},\ \delta_2^{WL}\mathbf{I_m},\ \cdots,\ \delta^{\mathbf{WL}}_{\mathbf{n_{beam}/2}}\mathbf{I_m})$$

Asymmetric stiffness perturbations

IV Additive uncertainty of $0.8 \cdot 10^2 \frac{N}{m^2}$ with respect to bending stiffness EI_{xx} for each tuning beam on the left wing and $1.2 \cdot 10^2 \frac{N}{m^2}$ for each tuning beam on the right wing

$$\mathbf{\Delta_K^{IV}} = \begin{bmatrix} \mathbf{\Delta_K}^{WR} & \\ & \mathbf{\Delta_K}^{WL} \end{bmatrix} \text{ where}$$
$$\mathbf{\Delta_K}^{WR} = \text{diag}(\delta_1^{WR}\mathbf{I_m},\ \delta_2^{WR}\mathbf{I_m},\ \cdots,\ \delta^{\mathbf{WR}}_{\mathbf{n_{beam}/2}}\mathbf{I_m}) \text{ and}$$
$$\mathbf{\Delta_K}^{WL} = \text{diag}(\delta_1^{WL}\mathbf{I_m},\ \delta_2^{WL}\mathbf{I_m},\ \cdots,\ \delta^{\mathbf{WL}}_{\mathbf{n_{beam}/2}}\mathbf{I_m})$$

V Additive uncertainty of $0.8 \cdot 10^2 \frac{N}{m^2}$ with respect to torsional stiffness GI_p for each tuning beam on the left wing and $1.2 \cdot 10^2 \frac{N}{m^2}$ for each tuning beam on the right wing

$$\mathbf{\Delta_K^{V}} = \begin{bmatrix} \mathbf{\Delta_K}^{WR} & \\ & \mathbf{\Delta_K}^{WL} \end{bmatrix} \text{ where}$$
$$\mathbf{\Delta_K}^{WR} = \text{diag}(\delta_1^{WR}\mathbf{I_m},\ \delta_2^{WR}\mathbf{I_m},\ \cdots,\ \delta^{\mathbf{WR}}_{\mathbf{n_{beam}/2}}\mathbf{I_m}) \text{ and}$$
$$\mathbf{\Delta_K}^{WL} = \text{diag}(\delta_1^{WL}\mathbf{I_m},\ \delta_2^{WL}\mathbf{I_m},\ \cdots,\ \delta^{\mathbf{WL}}_{\mathbf{n_{beam}/2}}\mathbf{I_m})$$

VI Additive uncertainty of $0.8 \cdot 10^2 \frac{N}{m^2}$ with respect to both bending stiffness EI_{xx} and torisonal stiffness GI_p for each tuning beam on the left and $1.2 \cdot 10^2 \frac{N}{m^2}$ for each tuning beam on the right wing

$$\mathbf{\Delta_K^{VI}} = \begin{bmatrix} \mathbf{\Delta_K}^{WR} & \\ & \mathbf{\Delta_K}^{WL} \end{bmatrix} \text{ where}$$
$$\mathbf{\Delta_K}^{WR} = \text{diag}(\delta_1^{WR}\mathbf{I_m},\ \delta_2^{WR}\mathbf{I_m},\ \cdots,\ \delta^{\mathbf{WR}}_{\mathbf{n_{beam}/2}}\mathbf{I_m}) \text{ and}$$
$$\mathbf{\Delta_K}^{WL} = \text{diag}(\delta_1^{WL}\mathbf{I_m},\ \delta_2^{WL}\mathbf{I_m},\ \cdots,\ \delta^{\mathbf{WL}}_{\mathbf{n_{beam}/2}}\mathbf{I_m})$$

Based on the above defined cases, robust aeroelastic analysis results are shown as μ-f plots at various flight speeds in figures 7-12. μ values are taken from the upper

bound calculation. The results for the robust flutter velocities and frequencies are summarized in Table 2. The columns in the are selfexplanatory. The flutter results for the nominal model is presented in Table 1.

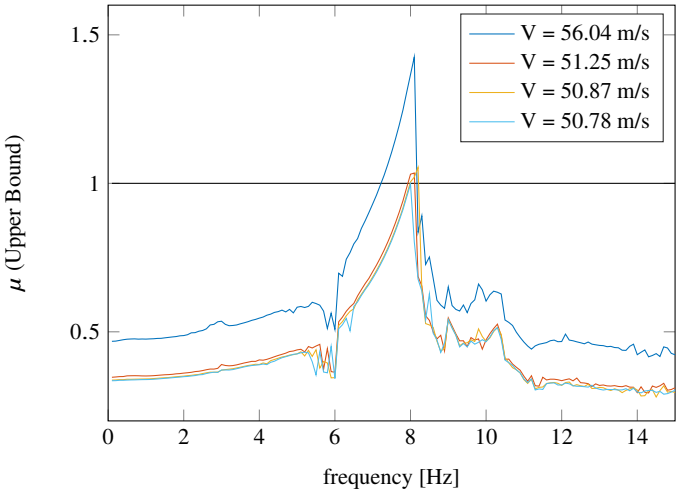

Fig. 7 μ-frequency plots of robust stability analysis for Case I

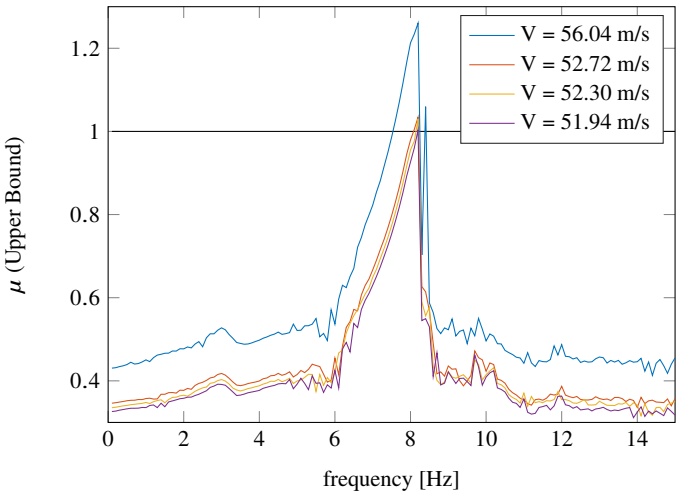

Fig. 8 μ-frequency plots of robust stability analysis for Case II

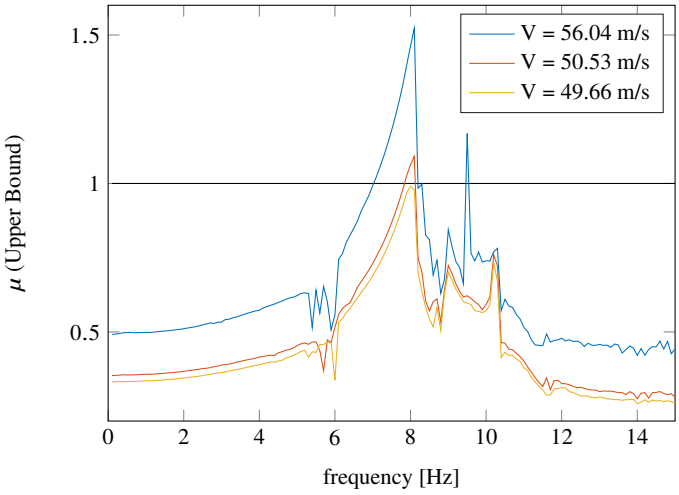

Fig. 9 μ-frequency plots of robust stability analysis for Case III

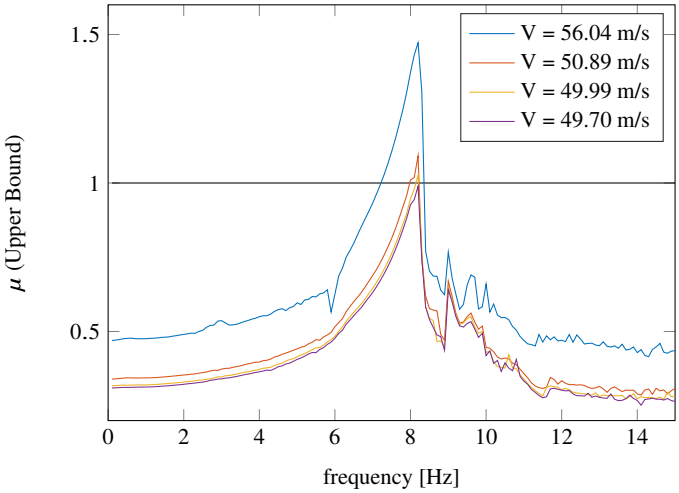

Fig. 10 μ-frequency plots of robust stability analysis for Case IV

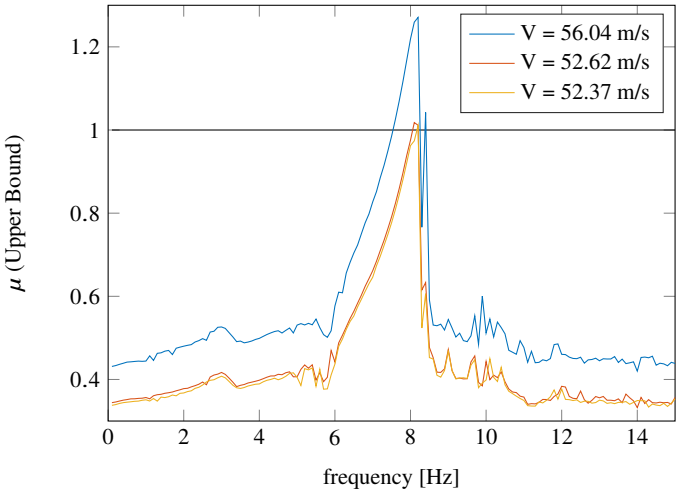

Fig. 11 μ-frequency plots of robust stability analysis for Case V

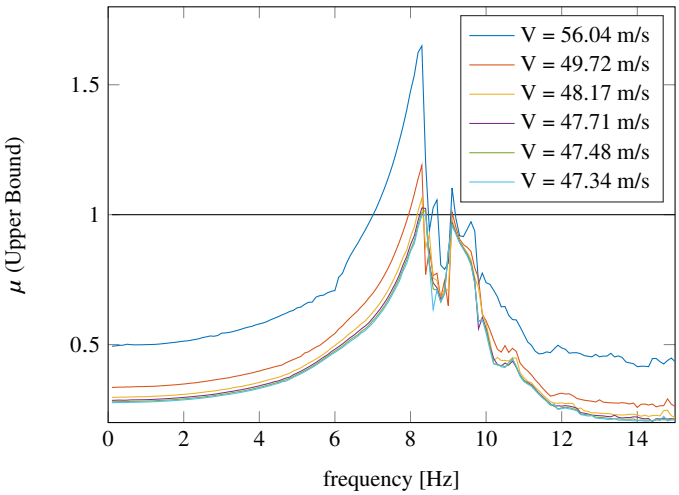

Fig. 12 μ-frequency plots of robust stability analysis for Case VI

Table 1 Comparison of nominal flutter analysis results

Method	Type	Aerodynamics	$f_{flutter}$ [Hz]	$V_{flutter}$ [m/s]
p	Nominal	quasi-steady	7.330	57.12
p	Nominal	unsteady	7.727	56.04

Table 2 Comparison of robust flutter analysis results

Case	Method	Type	Aerodynamics	$f_{flutter}$ [Hz]	$V_{flutter}$ [m/s]
I	μ-V	Robust	unsteady	8.00	50.78
II	μ-V	Robust	unsteady	8.20	51.94
III	μ-V	Robust	unsteady	8.00	49.66
IV	μ-V	Robust	unsteady	8.20	49.70
V	μ-V	Robust	unsteady	8.20	52.37
VI	μ-V	Robust	unsteady	8.40	47.34

7.1 Analysis results

The numerical example demostrates that even small stiffness parameter variations on the wing structures have a major impact on the onset of the flutter. There are considerable differences between flutter speeds with respect to bending and torsional stiffness variations. The impact of bending stiffness variations on the flutter margin is much stronger than the torsional stiffness uncertainties. The defined uncertainty in Case I reduces the flutter speed by roughly 9.4% compared to the nominal flutter speed given in Table 1 whereas the symmetric uncertainty of the torsional stiffness defined in Case II leads to a reduction of the flutter speed by roughly 7.3%. The Case III depicts a combination of the previous two cases. A further important point relating to key characteristics of the results refers to the asymmetry of the stiffness distribution as an uncertainty integrated into the nominal model. Comparison of the flutter speeds between CASE I and CASE IV leads to the conclusion that an asymmetric bending stiffness uncertainty has an greater influence on the flutter margin then an assumption of symmetric bending stiffness uncertainty, whereas the flutter speeds in CASE II and CASE IV related to the symmetric and asymmetric torsional stiffness uncertainties remain relatively unchanged. Comparison of the results between CASE III and CASE VI also reflects that a combination of asymmetric stiffness uncertaities related to bending and torsion parameters has a stronger effect on the flutter margin in comparison to the assumption of symmetric stiffness uncertaities in the model. Detailed results are shown in Table 2.

8 Conclusions

In this work a robust aeroelastic stability analysis within the μ-framework has been carried out. Therefore, a LFT model of the perturbated aeroelastic system in state-space form which is parametrized over flight speed, has been developed. Here, account is taken of the uncertainties in the structural stiffness model which has a significant impact within the lower frequency range and flutter analysis respectively. For the realization of the stiffness parameter variations tuning beams have been generated with respect to the condensed FE model. This approach is suitable for

varying of stiffness parameters by only adjusting material properties of the tuning beams avoiding to intervene the full FE model. The study is limited to the wings of the aircraft and focussed on the investigation of physical stiffness uncertainties of the wings in spanwise direction and handle each wing seperately in case of symmetric and especially asymmetric stiffness distribution which is widely underresearched scientifically with respect to robust aeroelastic analyses.

Acknowledgements The author wishes to thank Dr.ir. Gertjan Looye for supporting on specific issues relating to the μ-analysis used in this paper.

References

1. Lind, R., Brenner, Martin J.: Robust flutter margin analysis that incorporates flight data (1998)
2. Wuestenhagen, M., Kier, T., Meddaikar, Y., Pusch, M., Ossmann, D., Hermanutz, A.: Aeroservoelastic Modeling and Analysis of a Highly Flexible Flutter Demonstrator, Atmospheric Flight Mechanics Conference (2018)
3. Kier, T., Looye, G.: Unifying Manoeuvre and Gust Loads Analysis, International Forum on Aeroelasticity and Structural Dynamics, 2009